THE JOURNAL OF BIOLOGICAL CHEMISTRY VOL. 286, NO. 37, pp. 32843–32853, September 16, 2011

Metabolic Alterations in Highly Tumorigenic Glioblastoma Cells

PREFERENCE FOR HYPOXIA AND HIGH DEPENDENCY ON GLYCOLYSIS[*S]

Received for publication, May 14, 2011, and in revised form, July 22, 2011 Published, JBC Papers in Press, July 27, 2011, DOI 10.1074/jbc.M111.260935

Yunfei Zhou[‡], Yan Zhou[‡], Takashi Shingu[§], Li Feng[‡], Zhao Chen[‡], Marcia Ogasawara[‡], Michael J. Keating[¶], Seiji Kondo[§], and Peng Huang[‡1]

From the Departments of [‡]Molecular Pathology, [§]Neurosurgery, and [¶]Leukemia, The University of Texas M. D. Anderson Cancer Center, Houston, Texas 77030

Recent studies suggest that a small subpopulation of malignant cells with stem-like properties is resistant to chemotherapy and may be responsible for the existence of residual cancer after treatment. We have isolated highly tumorigenic cancer cells with 100-fold increase in tumor initiating capacity from the tumor xenografts of human glioblastoma U87 cells in mice. These cells exhibit stem-like properties and show unique energy metabolic characteristics including low mitochondrial respiration, increased glycolysis for ATP generation, and preference for hypoxia to maintain their stemness and tumor forming capacity. Mechanistically, mitochondrial depression in the highly tumorigenic cells occurs mainly at complex II of the electron transport chain with a down-regulation of the succinate dehydrogenase subunit B, leading to deregulation of hypoxia-inducible factors. Under hypoxia, the stem-like cancer cells are resistant to conventional anticancer agents but are sensitive to glycolytic inhibition. Furthermore, combination of glycolytic inhibition with standard therapeutic agents is effective in killing the tumor-initiating cells *in vitro* and inhibits tumor formation *in vivo*. Our study suggests that stem-like cancer cells prefer a low oxygen microenvironment and actively utilize the glycolytic pathway for ATP generation. Inhibition of glycolysis may be an effective strategy to eradicate residual cancer stem cells that are otherwise resistant to chemotherapeutic agents in their hypoxic niches.

Cancer cells are commonly regarded as an immortal cell population with unlimited life span, a trait that seems to resemble normal stem cells. However, recent studies suggest that only a small population of tumor-initiating cells with stem-like properties within a tumor are capable of long term self-renewal and generating the rapidly proliferating progenies that eventually form the tumor bulk (1–3). Because the persistence of tumor-initiating cells likely plays a major role in cancer development and disease recurrence after therapy, it is essential to understand their biological properties and to develop new anticancer agents and therapeutic strategies that are effective in killing the cancer stem cells (4–7). The stem-like cancer cells are thought to be intrinsically resistant to anticancer agents because of their high survival capacity (8–10), expression of drug resistance molecules such as multidrug-exporting pump ABCG2 (4), and the unique microenvironment (niche) in which they reside (11). It has been shown that tissue microenvironment may significantly affect normal stem cell function and differentiation. In particular, low O_2 level may promote the survival of normal stem cells and maintain their stemness as observed in the experimental models of hematopoietic stem cells, neural stem cells, and mouse embryonic stem cells (12–16). As such, it is possible that tumor-initiating cells are likely under the influence of the niche regulation and that these stem-like cancer cells may also prefer a hypoxic microenvironment. However, currently there are few experimental data on the metabolic properties of cancer stem cells, and the potential therapeutic implications are yet to be explored.

Human glioblastoma is the most frequent primary malignant brain tumor in adults and is among the most aggressive malignancies. Approximately half of the newly diagnosed glioblastoma patients are in the late stages and have poor prognosis. Although glioblastoma can be treated with surgery, radiotherapy, and chemotherapy, a majority of patients die within 2 years (17). In brain tumor tissues, hypoxia occurs in certain areas of the tumor bulk because of inadequate blood vessel supply. Such hypoxic tissue environment is also known to induce resistance to chemotherapy and radiation therapy and thus poses a major challenge in the clinical treatment of brain tumors (18). In addition, malignant brain tumor tissues display metabolic abnormality as reflected by increased uptake of glucose than normal brain tissues, and a high level of glucose utilization appears to be negatively associated with prognosis in patients with glioblastoma (19). More recently, it is reported that CD133+ cells, which are thought to contain brain tumor-initiating cells, are more resistant to radiation than the CD133-negative cells, implying that the subpopulation of stem-like cancer cells may be an important source of residual disease, leading to glioblastoma recurrence after treatment (3, 7).

Increased glucose uptake and high aerobic glycolysis in cancer cells have been known for more than half a century. Otto Warburg (20) first suggested that cancer cells might adapt the primitive glycolytic metabolic pattern of embryonic cells and that mitochondrial injury and metabolic switching to glycolysis might be essen-

* This work was supported, in whole or in part, by National Institutes of Health Grants CA085563, CA100428, CA109041, and CA16672. This work was also supported by an Odyssey Fellowship sponsored by the Houston Endowment.

[S] The on-line version of this article (available at http://www.jbc.org) contains supplemental text and Figs. S1 and S2.

[1] To whom correspondence should be addressed: Unit 951, 1515 Holcombe Blvd., Houston, TX 77030. Tel.: 713-834-6044; Fax: 713-834-6084; E-mail: phuang@mdanderson.org.

tial for cancer development. However, the metabolic properties of stem-like cancer cells and their relevance in cancer therapeutics remain poorly understood. We speculate that low mitochondrial function and high glycolytic activity may promote tumorigenicity and tumor progression in brain tumors. Such metabolic properties might confer advantage for the cancer cells to survive and grow in hypoxic tissue environment. In this study, we used a human glioblastoma experimental model to enrich stem-like tumor-initiating cells *in vivo*, characterized the energy metabolic properties of the isolate stem-like cancer cells *in vitro* under normoxia and hypoxia conditions, and tested their drug sensitivity *in vitro* and *in vivo*. A major goal was to identify new strategies that are effective in killing the stem-like cancer cells and overcome their drug resistance under hypoxia conditions.

EXPERIMENTAL PROCEDURES

Cell Culture and Tumor Xenografts—Human glioblastoma U87 cells were cultured in DMEM supplemented with 10% FBS at 37 °C in a humidified atmosphere with 5% CO_2. Tumor xenografts were generated by injecting U87 cells (2×10^6 cells/inoculum) subcutaneously into athymic nu/nu mice (Harlan, Madison, WI). U87-SC cells were isolated from the U87 tumor xenografts by physical dissociation of the tumor cells and maintained in brain tumor stem cell medium consists of a basal Dulbecco's modified Eagle's medium/F-12 (low glucose) supplemented with 5% fetal bovine serum, epidermal growth factor (20 ng/ml), basic fibroblast growth factor (20 ng/ml), pyruvate (1 mM), and uridine (50 μg/ml) under ambient oxygen concentration (21% oxygen) or hypoxic conditions (2% oxygen). Hypoxic culture conditions were created by incubating cells in a sealed modular incubator chamber (Billups-Rothenberg, Del Mar, CA) flushed with a gas mixture of 2% O_2, 5% CO_2, and 93% N_2.

Evaluation of in Vivo Tumorigenicity—To compare the tumorigenicity between U87 and U87-SC, different numbers of U87-SC cells ranging from 10^3 to 10^6 were inoculated on the right flanks of athymic nu/nu mice (Harlan) and the same numbers of regular U87 cells on the left flanks of the same mice subcutaneously to observe tumor growth for up to 100 days. To test the drug effect on tumor initiating capacity, U87-SC cells maintained in hypoxia were treated with various concentrations of drugs for 24 h as indicated, washed, and harvested for subcutaneous inoculation into athymic mice. Each inoculation site was injected with 3×10^5 cells. The mice were then monitored for tumor formation rate without further drug treatment *in vivo*. Intracranial inoculation of tumor cells and histology examination was done as previously described (21). All of the animal experiments were conducted in accordance with the guidelines for the use and care of laboratory animals and approved by the institutional animal care and use committee of the University of Texas M. D. Anderson Cancer Center.

3-(4,5-Dimethylthiazol-2-yl)-2,5-diphenyltetrazolium Bromide Assay—Cell growth inhibition was determined by MTT[2] assay in 96-well plates. Briefly, 3,000 cells were seeded in 96-well plates in 150 μl of medium containing final drug concentration at the first day. After 72 h of drug incubation, 50 μl of MTT reagents (3 mg/ml) were added to each well and incubated for 4 h. The formazan precipitates in the cells were dissolved in 200 μl of Me_2SO. Absorbance was determined using a MultiSkan plate reader (LabSystems, Helsinki, Finland) at 570 nm. Mitochondrial reductase activity was measured by the cleavage of MTT in a range of cells plated over 24 h.

Assay of Glycolytic Activity—The relative glycolytic activity in U87 and U87-SC cells was determined by measuring three major biochemical parameters: oxygen consumption, glucose uptake, and lactate production. For oxygen consumption assay, equal numbers of cells were suspended in 1 ml of fresh medium pre-equilibrated with fresh air (containing 21% oxygen and 5% CO_2) at 37 °C and transferred to a sealed respiration chamber equipped with a thermostat controller and a microstirring device (Oxytherm, Hansatech Instrument, Norfolk, UK). Oxygen concentration in the medium was then measured by the Clark-type oxygen electrode, following the manufacturer's recommended procedures. Oxygen consumption rate was expressed as nanomoles of O_2 consumed per min per 4 millions cells. Glucose uptake was measured using [^{3}H]2-deoxyglucose, and lactate production was measured using an Accutrend lactate analyzer to quantify lactate concentrations in the cell culture medium. Glycolytic index was calculated based on oxygen consumption, glucose uptake, and lactate production as described previously (22).

Measurement of Cellular ATP—Cellular ATP concentration was measured using the ATP-based CellTiter-Glo Luminescent Cell Viability kit (Promega, Madison, WI) modified from the manufacturer's protocol. Briefly, the cells were plated in 96-well plates at different densities to allow for attachment overnight. The next day, an equal volume of a single one-step reagent provided by the kit was added to each well and rocked for 15 min at room temperature. Cellular ATP content was measured using a luminescent plate reader. To test the ATP depleting effect of the glycolytic inhibitor, various concentrations of compound were added to the cells seeded at 5,000 cells/well for additional 24 h, and cellular ATP content was measured as described above.

Western Blot Analysis and Antibodies—The antibodies against CD133, nestin, lactate dehydrogenase, and pyruvate dehydrogenase were purchased from Abcam (Cambridge, MA). Hypoxia-inducible transcription factor (HIF)-1α antibody was purchased from BD Transduction (San Jose, CA). Glucose transporter (Glut)-1 antibody was purchased from Chemicon (Billerica, MA). HIF-2α and hexokinase II antibodies were from Santa Cruz Biotechnology, Inc. (Santa Cruz, CA). Antibodies against subunits of mitochondrial respiration complex I (20kd), complex II (SDHB), complex III (Core 2), and complex IV (Cox II) were purchased from Molecular Probes (Eugene, OR). Immunoblotting was performed using SDS-PAGE as previously described (22).

Immunofluorescence Staining—U87-SC neurospheres were cultured in microscopic glass chamber slides and fixed with 4% formaldehyde for 10 min at 4 °C. After blocking in PBS containing 2% BSA for 1 h at room temperature, the cells were stained with primary antibodies against CD133 (Miltenyi, Auburn, CA)

[2] The abbreviations used are: MTT, 3-(4,5-dimethylthiazol-2-yl)-2,5-diphenyltetrazolium bromide; P-BrPE, pentyl 3-bromopyruvate ester; OCR, oxygen consumption rate; HIF, hypoxia-inducible factor; SDHB, succinate dehydrogenase subunit B; NAC, *N*-acetylcysteine; ROS, reactive oxygen species; Glut, glucose transporter; BCNU, bis-chloroethylnitrosourea.

or nestin (Abcam) and a secondary goat anti-mouse IgG-FITC according to the manufacturer's guide. Fluorescent images were visualized and captured using a Nikon fluorescent microscope with proper filter set.

Reverse Transcriptase-PCR—Total RNA was isolated using a RNA extraction kit (Qiagen). cDNA was synthesized from RNA using Superscript™ first strand synthesis system for RT-PCR (Invitrogen) according to the manufacturer's guide. The primer sequences used to amplify human CD133 and actin genes are described in the supplemental materials.

Flow Cytometry Analysis—Cellular ROS level was detected by incubating live cells with redox-sensitive probe dichlorofluorescein diacetate (DCFDA) or hydroethedium (Molecular Probes) at the manufacturer's recommended concentration for 1 h followed by analysis using a FACSCalibur flow cytometer (BD Biosciences). CD133 expression was assessed by flow cytometer using an anti-CD133/1 antibody (clone 293C3, Miltenyi) and a secondary goat anti-mouse IgG-FITC antibody according to the manufacturer's guide. Mouse IgG1-FITC was used as a negative control. Propidium iodide (10 μl/ml) staining was used to reveal dead cells.

Anchorage-dependent and -independent Colony Formation Assays—For anchorage-dependent colony formation, the cells were seeded into 6-well plates at 800 cells/well in the desired medium containing the indicated concentrations of drugs and incubated at 37 °C under normoxia (21% oxygen) or hypoxia (2%) for 2 weeks. Colonies were photographed and counted. Anchorage-independent colony formation assay was performed using double-layer soft agar in 6-well plates with a top layer of 0.35% agar and a bottom layer of 0.7% agar modified from a previously described bioassay for human tumor stem cells (23). Briefly, the cells maintained in normoxia or hypoxia were treated with various concentrations of drugs for 24 h, and the attached cells were trypsinized, and 1,000 cells from different treatment condition were suspended in 0.35% agar medium and laid on the top of the supporting agar layer. Colonies were allowed to form in an incubator at 37 °C for 21 days, stained, and counted.

Drug Efficacy Evaluation by in Vivo Xenograft Model—To evaluate the *in vivo* therapeutic activity of pentyl 3-bromopyruvate ester (P-BrPE), doxorubicin, BCNU (bis-chloroethylnitrosourea), and their combinations in mice bearing glioblastoma U87-SC cells (without any drug treatment *in vitro*) were inoculated subcutaneously at both flanks of athymic mice (3×10^5 cells/injection site). When the tumor xenografts were established and measurable 7 days after inoculation, the mice were randomly divided into six groups for the following treatment: 1) control group treated with solvent only; 2) P-BrPE: 20 mg/kg, intravenously (via tail vein), three times per week (Monday, Wednesday, and Friday) for the first 3 weeks, followed by once per week maintenance treatment each Monday until the first mice required euthanasia because of excessive tumor burden as mandated by the institutional animal care and use committee protocol; 3) doxorubicin: 2 mg/kg, intraperitoneal, twice per week (Monday and Friday) for the first 3 weeks, followed by once per week maintenance treatment each Monday until the first mouse required euthanasia; 4) combination of P-BrPE and doxorubicin as specified in groups 2 and 3; 5) BCNU: 20 mg/kg, intraperitoneal, twice per week (Monday and Friday) for the first 3 weeks, followed by once per week maintenance treatment for 3 weeks (weeks 4, 5, and 6) and then twice per week treatment (Monday and Friday) until the first mouse required euthanasia because of excessive tumor burden; and 6) combination of P-BrPE and BCNU using the dose schedule as specified in group 5. Doxorubicin and BCNU were purchased from Sigma. P-BrPE was synthesized by esterification of 3-bromopyruvate (Sigma) with 1-pentanol (Sigma). For *in vivo* drug administration, P-BrPE was first diluted in ethanol and then formulated as injectable (intravenously) solution in 25% hydroxypropyl β-cyclodextrin (Cyclodextrin Technologies, Gainesville, FL) in PBS.

RESULTS

In Vivo and in Vitro Microenvironment Selected for Neurosphere-forming U87-SC Cells with High Tumor Initiating Capacity—To obtain cancer cells with enriched tumor-initiating cells, we inoculated human glioblastoma U87 cells into nude mice subcutaneously for tumor xenograft formation and then harvested cancer cells from the tumor mass (Fig. 1*A*). Cells freshly isolated from the tumor xenograft were maintained in brain tumor stem cell medium under normoxia (ambient oxygen) or hypoxia (2% oxygen). This experimental design was based on the notion that physiologic oxygen tension *in vivo* is ~2–9% (24), and stem-like cancer cells can be enriched under hypoxic environment (12, 13). We observed a striking difference in morphology between *in vivo* selected U87 cells and the parental U87 cells. At similar seeding density, cells isolated from xenograft and maintained in brain tumor stem cell medium formed many neurosphere-like cell clusters under hypoxic conditions, whereas the parental U87 cells mainly proliferated as a monolayer (Fig. 1*B*). The sphere formed in hypoxia seems to resemble the typical neural stem cell morphology (25). Interestingly, when a single sphere isolated from the primary culture derived from tumor xenograft was trypsinized and subcultured under hypoxic conditions, many secondary spheres formed. These spheres could be expanded and maintained in spheroid stage in long term culture. In contrast, when cells from a single sphere were trypsinized and cultured under normoxic conditions, the cells grew in monolayer (Fig. 1*B*). We further characterized these cells for their expression of the putative cancer stem cell surface markers CD133 and nestin and found both markers increased (see below). We designated the cells isolated from the U87 xenograft as U87-SC cells. Theses cells seemed to prefer hypoxic environment to maintain their unique cell-cell interaction in stem-like sphere stage.

To functionally evaluate the tumorigenic property of U87-SC cells, we compared the *in vivo* tumor formation capacity of U87-SC cells and the parental U87 cells. Various numbers of U87-SC cells (maintained under hypoxia in spheroid stage and trypsinized before inoculation) were injected subcutaneously on the right flanks of athymic nude mice (10^3–10^6 cells/injection site), and the same numbers of parental U87 cells were inoculated on the opposite flanks. As illustrated in Fig. 1*C*, U87-SC cells exhibited high capacity to form tumors *in vivo* with as low as a 10^4 cells/inoculation, whereas 10^6 of parental U87 cells were required to generate a tumor. At 10^6 cells/inoc-

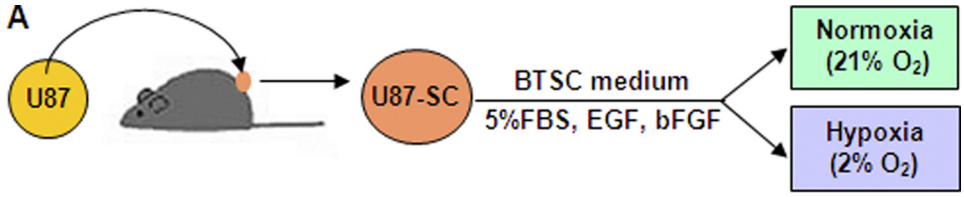

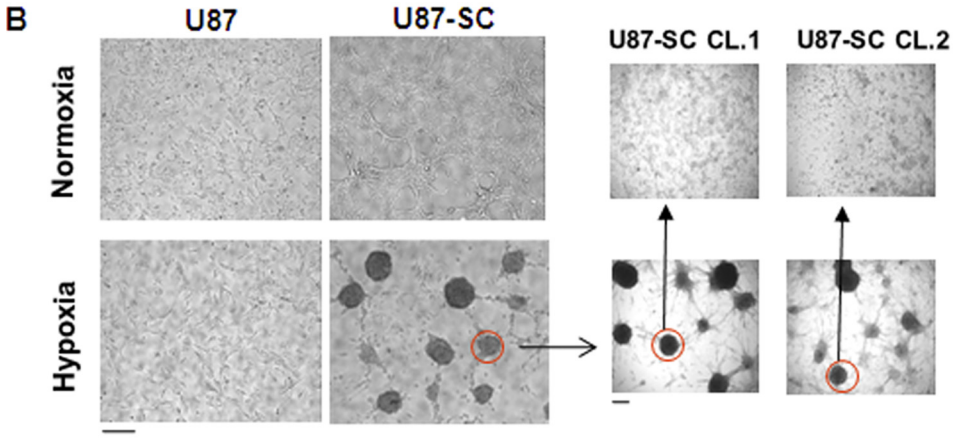

C

Cell type	Cells inoculated	Tumor Incidence	Median latency (day)
U87 (normoxia)	1x 10^3	0/4	n/a
	1x 10^4	0/4	n/a
	1x 10^5	0/4	n/a
	1x 10^6	3/4	12 (8, 12, 19)
U87-SC (hypoxia)	1x 10^3	0/4	n/a
	1x 10^4	1/4	68
	1x 10^5	4/4	10 (8, 10, 10, 12)
	1x 10^6	4/4	9 (8, 9, 10,10)

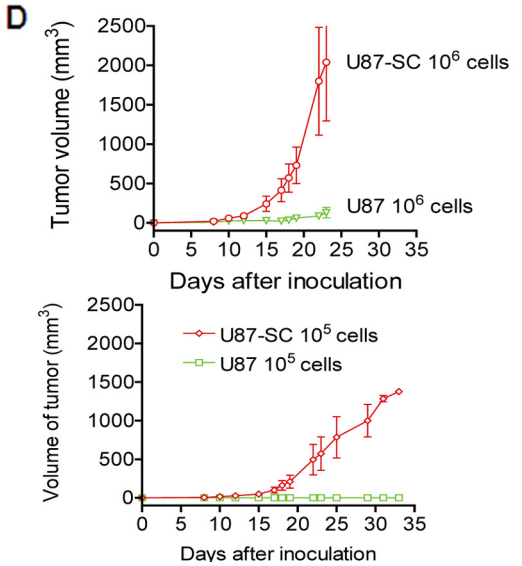

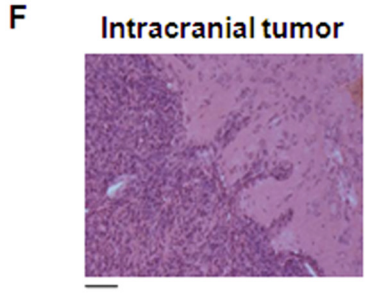

FIGURE 1. **Isolation of tumor cells from human glioblastoma xenografts (U87-SC) and characterization of its tumorigenicity.** *A*, experimental schema for generating U87 tumor xenografts and establishment of U87-SC cell model. *B*, unique morphology of primary and secondary neurosphere formation in U87-SC cells under hypoxic conditions. *C*, increased tumor incidence and decreased tumor latency of hypoxic U87-SC cells compared with normoxic U87 cells ($n = 4$). *D*, tumor xenograft growth curves of mice inoculated with U87 and U87-SC cells at 10^5 or 10^6 cells/site. *E*, images of nude mice bearing U87 (*left*) and U87-SC (*right*) xenografts with 10^6 cell/site at day 30. *F*, Hematoxylin and eosin staining of brain tissue from a mouse bearing xenograft of U87-SC cells inoculated orthotopically. *Bar*, 50 μm.

ulum, the U87-SC xenografts showed a median latency of 9 days (*versus* 12 days for U87 cells; $p > 0.05$, not statistically significant) and a more rapid tumor growth compared with U87 xenografts (Fig. 1, *D* and *E*). Moreover, intracranial inoculation of U87-SC cells led to aggressive tumor formation in all mice, whose tumors appeared highly invasive with multiple infiltrating tumor cell clusters in the brain tissue (Fig. 1*F*) and formation of metastatic foci (not shown). Thus, U87-SC cells represented a unique subpopulation of highly tumorigenic cells that were selected through *in vivo* tumor formation and further enriched *in vitro* under stem cell culture conditions and hypoxic microenvironment.

U87-SC Cells Exhibited Stem-like Properties and Drug Resistance Phenotype—To further characterize the highly tumorigenic U87-SC cells, we examined their self-renewal capacity and expression of neural stem cell markers. Consistent with their high tumorigenicity *in vivo*, U87-SC cells exhibited higher capacity to form colonies than U87 cells (Fig. 2*A*). Intriguingly, hypoxia promoted colony formation in both cell lines, with U87-SC cells forming significantly more colonies. Comparison of the cell growth curves by direct counting of cell numbers revealed that U87-SC cells have similar growth rate as U87 cells under normoxia, whereas U87-SC cells proliferated better under hypoxic conditions (Fig. 2*B*). Because colony formation capacity is an indicator of long term cellular self-renewal potential (23), these observations indicate that U87-SC cells have a higher self-renewal capacity than U87 cells, and hypoxia seemed to increase self-renewable population in both U87 and U87-SC cells.

The neurosphere-like structures of the U87-SC cells under hypoxic conditions indicate that these cells may contain stem-like properties. We then examined the expression of putative brain tumor stem cell markers in U87 and U87-SC cells. Of note, U87 cells were shifted from normoxia to hypoxia for 72 h before RNA isolation and protein extraction. U87-SC cells were maintained in long term hypoxia or long term normoxia for comparison. As shown in Fig. 2*C*, higher expression of CD133 mRNA was observed in U87-SC cells, and the expression levels of CD133 mRNA and protein were further enhanced by hypoxia. Furthermore, the U87-SC cells contain elevated levels of nestin, a neural stem cell marker, in both normoxic and hypoxic conditions. Consistently, flow cytometry analysis of U87-SC cells stained with an anti-CD133 antibody revealed that there was an approximately 2-fold increase of CD133+ subpopulation under the hypoxic conditions (Fig. 2*D*). Immunofluorescent staining showed a heterogeneous expression of CD133 among the cells within a sphere and an intense expression of the neural stem cell marker nestin in cells near the surface of the spheres (Fig. 2*E*).

Because it has been speculated that stem-like cancer cells are resistant to anticancer agents in part because of their high capacity to export drugs out of the cells and high expression of cell survival molecules (8, 9), we tested the sensitivity of U87-SC cells to anticancer agents. As shown in Fig. 2*F*, U87-SC cells were less sensitive to BCNU or doxorubicin compared with the parental U87 cells. This drug-resistant phenotype was observed in both normoxia and hypoxia, with U87-SC cells being more resistant to each drug under hypoxic conditions, as evidenced

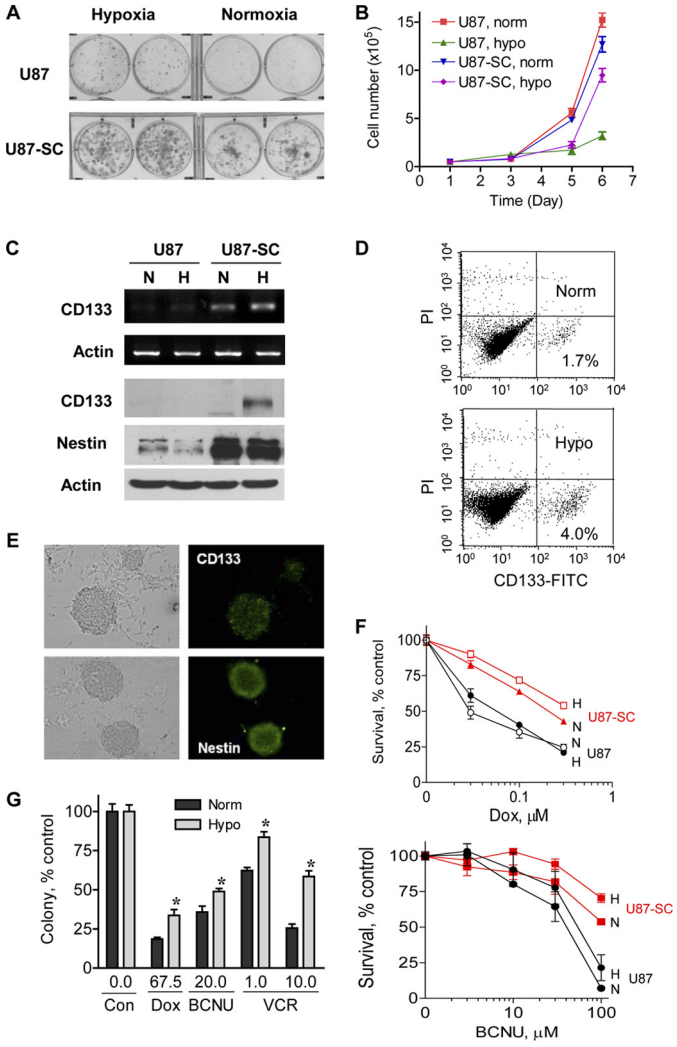

FIGURE 2. **U87-SC cells showed enhanced expression of neural stem cell markers and resistance to conventional anticancer agents under hypoxia.** *A*, increased anchorage-dependent colony formation of U87-SC cells under normoxia and hypoxia. Approximately 800 cells/well were seeded for both U87 and U87-SC cells and incubated for 12 days. *B*, cell growth curve of U87 and U87-SC cells under normoxia (*norm*) and hypoxia (*hypo*) seeded at 10,000 cells/well in 12-well plate ($n = 3$). *C*, RT-PCR analysis of CD133 mRNA expression and Western blot analysis of CD133 and nestin expression. *N*, normoxia; *H*, hypoxia. *D*, flow cytometry analysis of CD133+ subpopulation in U87-SC cells cultured under hypoxic or normoxic conditions. *Norm*, normoxia; *Hypo*, hypoxia. *E*, expression of CD133 and nestin in U87-SC cells of neurospheres detected by immunofluorescence staining. *Bar*, 50 μm. *F*, comparison of U87 and U87-SC cells for their sensitivity to doxorubicin (*Dox*) and BCNU under normoxia (*N*) or hypoxia (*H*) conditions, measured by MTT assay (72 h of drug incubation, $n = 3$). *G*, anchorage-dependent colony formation assay of U87-SC cells under treatment of doxorubicin (*Dox*, nM), BCNU (μM), or vincristine (*VCR*, nM) at the indicated drug concentrations. Colonies were allowed to form for 2 weeks (*error bar*, S.D.; $n = 3$; *, $p < 0.05$, normoxia *versus* hypoxia). *Norm*, normoxia; *Hypo*, hypoxia; *Con*, control.

by the higher IC_{50} values (supplemental Table S2). Colony formation assay demonstrated that hypoxia further enhanced the resistance of U87-SC cells to doxorubicin, BCNU, and vincristine (Fig. 2*G*), suggesting that the malignant cells might be resistant to multiple therapeutic agents in the hypoxic niches. Overall, the high ability of U87-SC cells to form neurospheres, to generate colonies under hypoxia, to increase CD133 and nestin expression, and to efficiently form tumors *in vivo* indicates that these cells were enriched in tumor-initiating cells with stem-like properties.

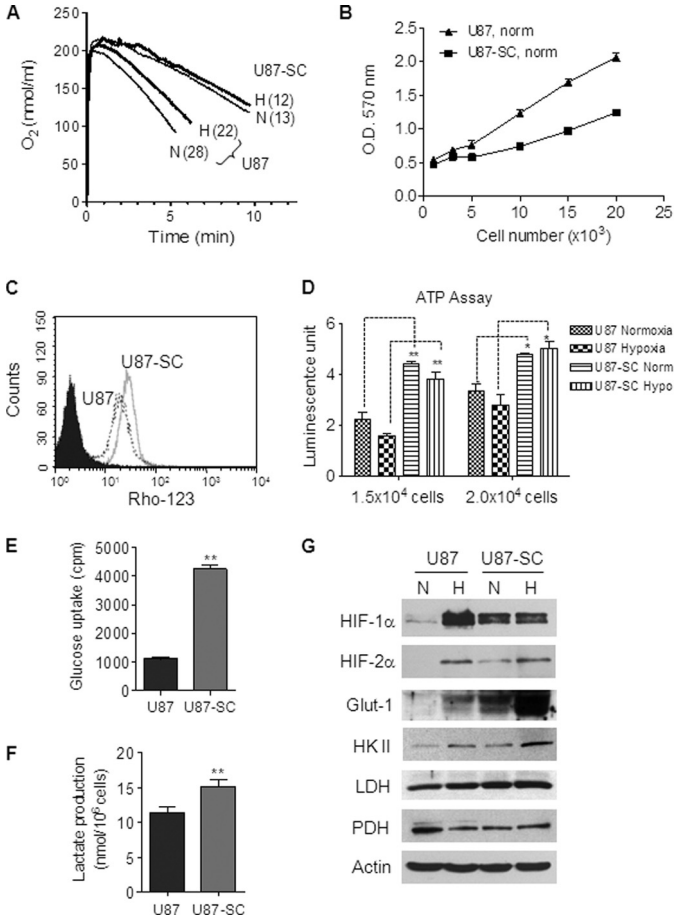

FIGURE 3. **U87-SC cells showed low mitochondrial respiration and elevated glycolysis.** *A*, comparison of mitochondrial respiration of U87 cells and U87-SC cells measured by oxygen consumption rate (*numbers* in *parentheses*, nmol/min/4 × 10^6cell/ml). Representative data are shown from three separate experiments. *B*, measurement of mitochondrial redox capacity of U87 and U87-SC cells by the mitochondrial reduction of MTT under normoxia ($n = 3$). *C*, comparison of mitochondrial membrane potential in U87 and U87-SC cells by rhodamine 123 uptake using flow cytometry analysis. *D*, measurement of total cellular ATP content in normoxic and hypoxic U87 and U87-SC cells (*error bar*, S.D.; $n = 3$; *, $p < 0.05$; **, $p < 0.01$, U87 *versus* U87-SC). U87 cells were switched to hypoxia for 72 h before measurement. *Norm*, normoxia; *Hypo*, hypoxia. *E*, measurement of glucose uptake in U87 and U87-SC cells (*error bar*, S.D.; $n = 3$; **, $p < 0.01$). *F*, comparison of lactate production in U87 and U87-SC cells ($n = 3$; **, $p < 0.01$). *G*, Western blot analysis of HIF-1α, HIF-2α, Glut-1, HKII, lactate dehydrogenase, and pyruvate dehydrogenase in U87 and U87-SC cells under normoxia (*N*) and hypoxia (*H*). U87 cells were maintained in normoxia and shifted to hypoxia for 72 h; U87-SC cells were continuously maintained in normoxia or hypoxia.

Low Mitochondrial Respiration and Up-regulation of Glycolysis in Stem-like Cancer Cells—The preference of U87-SC cells to hypoxic conditions to maintain their spheroid structures and expression of CD133 suggests a possible interaction between these cells and the oxygen environment. This prompted us to investigate the mitochondrial respiration activity using oxygen consumption rate (OCR) as a biochemical parameter. As shown in Fig. 3*A*, U87-SC cells displayed a 50% decrease in OCR compared with U87 cells, which was consistently observed when the cells were maintained in normoxic or hypoxic conditions prior to the oxygen consumption assays. These data suggest that the low mitochondrial respiratory activity might be an intrinsic property of U87-SC cells and was not due to culture under hypoxic conditions. To examine whether the decreased mitochondrial respiration in U87-SC cells was associated with abnormalities in mitochondrial morphology or a decrease in mitochondrial number, we used transmission electron microscopic analysis to examine the mitochondria of U87 and U87-SC cells. No obvious abnormalities in mitochondrial ultramicroscopic structure were observed in U87-SC cells (supplemental Fig. S1*A*). However, the density of mitochondria appeared increased in U87-SC cells, suggesting that the mitochondrial mass might be increased in U87-SC cells. This was confirmed by flow cytometry analysis for mitochondrial mass, using MitoTracker green and MitoTracker red staining (supplemental Fig. S1*B*). It is possible that the increase in mitochondrial mass in U87-SC cells was a compensatory response to the decreased mitochondrial respiratory activity. The decrease in mitochondrial function in U87-SC cells was also demonstrated by a significant decrease in their ability to convert MTT to a purple formazan (Fig. 3*B*). Of note, conversion of MTT is widely used for cell proliferation assay, although it was originally adopted as a functional analysis of mitochondrial reductase activity (26). Furthermore, the decreased mitochondrial function in U87-SC cells was also reflected by a lower mitochondrial membrane potential as measured by rodmine-123 staining in comparison with U87 cells (Fig. 3*C*).

When we compared the cellular ATP levels in U87 and U87-SC cells under normoxia and hypoxia conditions, we observed that the low mitochondrial respiration in U87-SC cells did not result in lower cellular ATP. In fact, U87-SC cells consistently showed a significant increase of cellular ATP compared with U87 cells under both normoxia and hypoxia conditions in multiple measurements with various cell numbers (Fig. 3*D*), suggesting that mitochondrial respiration might not be the major pathway for ATP generation in U87-SC cells. Because cells can generate ATP through glycolysis and mitochondrial oxidative phosphorylation, we next investigated the glycolytic pathway for ATP production in U87-SC cells. Indeed, U87-SC cells exhibited a 4-fold increase in glucose uptake (Fig. 3*E*) and an elevated lactate production in comparison with U87 cells under normoxic conditions (Fig. 3*F*). Using the three major biochemical parameters (oxygen consumption, glucose uptake, and lactate production) for estimating glycolytic activity (22), we calculated that the ratio of glycolytic indexes for U87 and U87-SC cells was 1:11, indicating that U87-SC cells had ~10-fold higher glycolytic activity than the parental U87 cells. Furthermore, analysis of several key molecules involved in energy metabolism showed that Glut-1 (a major glucose transporter) and hexokinase II (HK II, a key enzyme for the initial step of glycolysis) were up-regulated in U87-SC cells, especially under hypoxia (Fig. 3*G*). The expression of lactate dehydrogenase, which converts pyruvate to lactate during glycolysis, was also moderately increased. On the other hand, pyruvate dehydrogenase, a key mitochondrial enzyme that converts pyruvate to acetyl-CoA for further metabolism through the TCA cycle, was down-regulated in U87-SC cells (Fig. 3*G*).

Considering that these key metabolic enzymes are under the regulation of the HIF, we examined the status of HIF-1α and HIF-2α and found that both molecules were readily detectable in U87-SC cells under normoxic conditions (Fig. 3*G*). In contrast, the parental U87 cells showed little expression of HIF-1α

and HIF-2α in normoxia, and both molecules were up-regulated by hypoxia. Interestingly, although the basal HIF-1α was stabilized in U87-SC cells under normoxia, it did not further increase when the cells were exposed to hypoxic conditions. On the other hand, HIF-2α level was detectable in normoxic U87-SC cells and showed a further increase in hypoxic conditions. The increased stability of HIF-1α and HIF-2α proteins in U87-SC cells might be due in part to the increased generation of ROS in these cells (see below).

Decreased Mitochondrial Complex II Activity and Increased ROS Generation in U87-SC Cells—To explore the underlying mechanisms of decreased mitochondrial respiration in U87-SC cells, we first examined the expression of the mitochondrial respiratory chain components, using antibodies specific for the representative subunit of each mitochondrial electron transport complex (I, II, III, and IV) by Western blot analysis. As shown in Fig. 4*A*, there was a down-regulation of succinate dehydrogenase subunit B (SDHB) in U87-SC cells. SDHB is a subunit of complex II and a putative tumor suppressor gene (27). In contrast, there was no detectable change in expression of the subunits for complexes I, III, and IV in U87-SC cells compared with the parental U87 cells.

The down-regulation of SDHB in U87-SC cells prompted us to compare the functional activity of the mitochondrial complex I and II in terms of their contribution to the overall cellular oxygen consumption. We used a specific complex I inhibitor rotenone to differentiate the activities of complexes I and II. Oxygen consumption in U87 cells and U87-SC cells was measured before and after the addition of rotenone. The complex I activity was the portion of oxygen consumption that could be blocked by rotenone, whereas the remaining oxygen consumption represented the electron transport activity from complex II to the downstream complexes. As shown in Fig. 4*B*, the overall oxygen consumption was 50% lower in U87-SC cells, consistent with the observation in Fig. 3*A*. Importantly, addition of the complex I inhibitor rotenone blocked >80% of oxygen consumption in U87-SC cells, suggesting that the intrinsic complex II activity in these cells was low (<20% of total OCR). In contrast, ~40% of oxygen consumption remained after the addition of rotenone to the parental U87 cells. By subtracting the complex II OCR from the total OCR, the activity of complex I (OCR = ~12 ± 1) was comparable between U87 and U87-SC cells. These data, together with the observation of down-regulation of SDHB protein in U87-SC cells, suggested that a defect in complex II activity was likely the main reason for the lower mitochondrial respiration of U87-SC cells.

Recently, it was reported that HIF-1α and HIF-2α proteins could be stabilized under normoxia when SDHB was stably knocked down, leading to an increase in cellular ROS (28). Consistently, we also observed a 2-fold increase in both superoxide and hydrogen peroxide levels in U87-SC cells compared with U87 cells (Fig. 4*C*). This increase in ROS might be a consequence of mitochondrial dysfunction leading to increased electron leakage. Interestingly, treatment of U87-SC cells with 1 mM of *N*-acetylcysteine (NAC), an anti-oxidant precursor of GSH, led to a time-dependent decrease of ROS detected by a decrease of dichlorofluorescein diacetate signal (measurement for H_2O_2) and hydroethedium (measurement for O_2^-) as shown

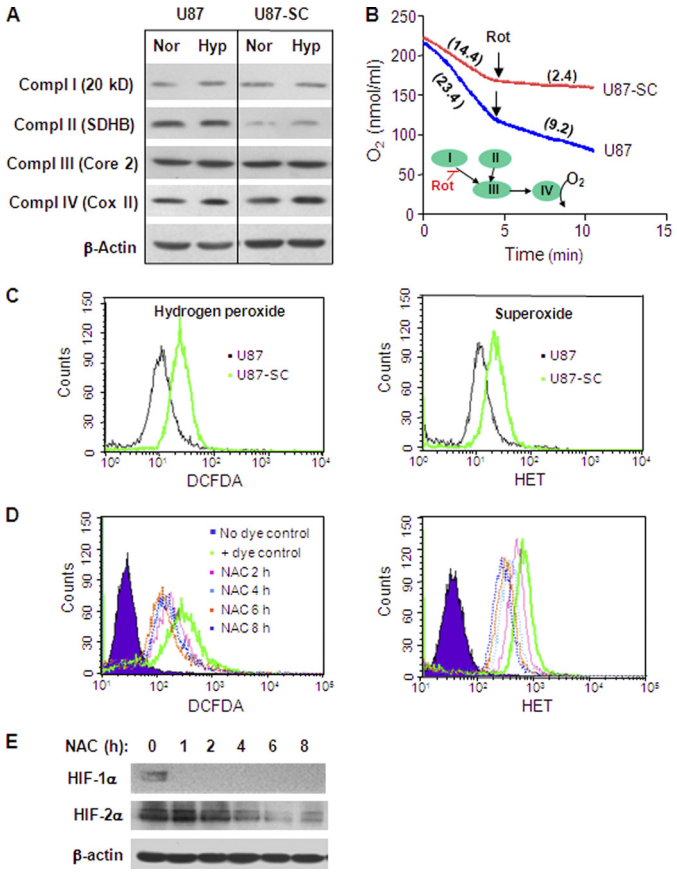

FIGURE 4. **U87-SC cells showed decreased mitochondrial respiratory complex II activity, increased ROS, and stabilization of HIF under normoxia.** *A*, Western blot analysis of subunits of mitochondrial respiratory complex I (20kd), complex II (*SDHB*), complex III (*Core 2*), and complex IV (*Cox II*), HIF-1,2α in U87 and U87-SC cells under normoxia (*Nor*) and hypoxia (*Hyp*). Actin was used as internal control. *B*, measurement of OCR in the presence or absence of 100 nM rotenone (*Rot*), a complex I inhibitor (*right*). The complex II activity was reflected by oxygen consumption rate (*numbers* in *parentheses*, nmol/min/4 × 10^6cell/ml) after adding rotenone to the cell suspension. The *inset* shows electron flow and the site of rotenone inhibition. Representative data were shown from three separate experiments. *C*, measurement of cellular ROS level using specific probe for hydrogen peroxide (*right panel*) and superoxide (*left panel*) in U87 and U87-SC cells under normoxia. *D*, measurement of cellular ROS level using specific probe for hydrogen peroxide (dichlorofluorescein diacetate, *DCFDA*) and superoxide (hydroethedium, *HET*). *E*, Western blot analysis of HIF-1α and HIF-2α protein levels of normoxic U87-SC cells treated with 1 mM NAC for 2–8 h.

in Fig. 4*D*. As a consequence of ROS decrease in the presence of NAC, HIF-1α and HIF-2α in U87-SC cells became unstable and diminished in normoxic culture (Fig. 4*E*). Thus, it appeared that HIF-1α and HIF-2α proteins in U87-SC cells might be stabilized in normoxia through a ROS-mediated mechanism, which might be attributed to ROS inhibition of prolyl hydroxylase (29). The increased basal levels of HIF in U87-SC cells might in turn promote glycolysis by up-regulation of Glut-1 and glycolytic enzyme (HKII) and suppression of the pyruvate utilization in the mitochondria by lowing pyruvate dehydrogenase expression, with an increased conversion of pyruvate to lactate through up-regulation of lactate dehydrogenase.

Highly Tumorigenic U87-SC Cells Were Sensitive to Glycolytic Inhibition in Vitro—Because we observed that U87-SC cells are likely under the influence of the hypoxic niche regulation and that these stem-like cancer cells exhibit a resistant

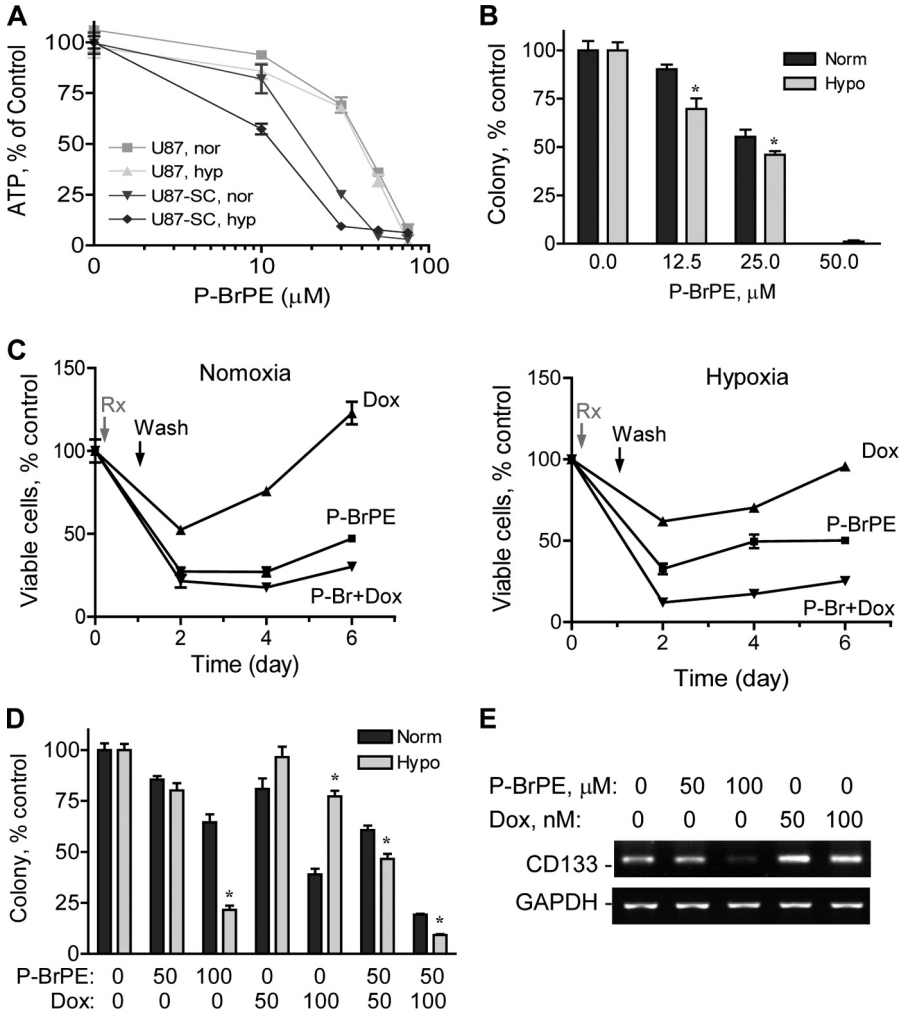

FIGURE 5. **Glycolytic inhibition abolished the growth of residual cancer cells *in vitro* and suppressed tumor formation and growth *in vivo*.** *A*, measurement of cellular ATP change after glycolytic inhibition by P-BrPE treatment for 16 h using Promega ATP assay kit ($n = 3$). *nor*, normoxia; *hyp*, hypoxia. *B*, inhibition of anchorage-dependent colony formation of U87-SC cells by P-BrPE under normoxia (*Norm*) or hypoxia (*Hypo*) (*error bar*, S.D.; $n = 3$; *, $p < 0.05$, normoxia *versus* hypoxia). *C*, assessment of residual cell regrowth by MTT assay after U87-SC cells were treated with P-BrPE (50 μM), doxorubicin (*Dox*, 500 nM), or their combination for 24 h followed a wash-off and supplementation with fresh medium under normoxia or hypoxia ($n = 3$). *D*, measurement of anchorage-independent colony formation of U87-SC cells in soft agar by 24 h of pretreatment of P-BrPE, doxorubicin (*Dox*), or the combination (*error bar*, S.D.; $n = 3$; *, $p < 0.05$, normoxia *versus* hypoxia). *E*, RT-PCR analysis of CD133 mRNA expression in hypoxic U87-SC cells after P-BrPE or doxorubicin (*Dox*) treatment for 24 h, followed by a 48-h recovery period cultured in fresh medium without drug.

phenotype to standard chemotherapeutic agents especially under hypoxic conditions (Fig. 2*F*), it is important to seek more effective means to kill the stem-like cancer cells. Considering the low mitochondrial respiration and high glycolytic phenotype of U87-SC cells, we hypothesized that inhibition of glycolysis would severely abolish their energy metabolism and might preferentially kill these stem-like cancer cells. Previous studies showed that 3-bromopyruvate and its derivatives inhibited glycolysis and caused severe ATP depletion in cancer cells (22, 30). Thus, we used a derivative of 3-bromopyruvate, P-BrPE to compare its effect on cellular ATP and cell viability in U87 and U87-SC cells under normoxic and hypoxic conditions. As shown in Fig. 5*A*, P-BrPE induced a concentration-dependent ATP depletion in both cell lines, with more potent effect on U87-SC cells, especially under hypoxia. The IC_{50} values for ATP depletion in U87-SC cells were 18.5 and 11.8 μM under normoxia and hypoxia, respectively. Colony formation assay showed that P-BrPE was potent in inhibiting U87-SC cells (Fig. 5*B*), with the IC_{50} values of 27.1 and 22.2 μM under normoxia and hypoxia, respectively. This was in contrast to the drug resistance phenotype with higher IC_{50} values when the cells were treated with conventional chemotherapy agents under hypoxia (Fig. 2, *F* and *G*).

The stem-like cancer cells are thought to be intrinsically resistant to anticancer agents because of their high survival capacity (8–10). Thus, strategies to eliminate this subpopulation of cells may provide important thearapeutic strategy to prevent disease recurrence. In a modified MTT assay, we tested the effect of P-BrPE on the regrowth of residual cancer cells after drug wash-off. As illustrated in Fig. 5*C*, U87-SC cells treated with doxorubicin (500 nM) showed 50 and 70% cell viability by in normoxia and hypoxia, respectively. The residual cells readily proliferated after the drug was washed off. Combination of P-BrPE and doxorubicin was able to largely block the regrowth of the residual cells under both normoxic and hypoxic conditions. Furthermore, an anchorage-independent colony

formation assay was used to compare the effect of P-BrPE and doxorubicin on the long term cell proliferation and self-renewal ability in soft agar. As shown in Fig. 5*D*, U87-SC cells were more resistant to doxorubicin in hypoxia than in normoxia, whereas P-BrPE exhibited more potent activity in hypoxia than in normoxia. Significantly, combination of subtoxic concentrations of doxorubicin and P-BrPE synergistically inhibited colony formation of U87-SC cells under hypoxia. For instance, 50 μM P-BrPE and 100 nM doxorubicin (24 h treatment) reduced U87-SC colony formation to 80 and 77% of the control, respectively. Combination of the two compounds eliminated most colonies (9% of control), significantly more toxic than the expected additive effect of 62% cell survival ($0.8 \times 0.77 = 0.62$).

Analysis of CD133 expression revealed that treatment of U87-SC cells with doxorubicin for 24 h followed by a 48-h recovery in drug-free medium led to an increase of CD133 expression, whereas incubation with P-BrPE in a similar fashion resulted in a substantial decrease in CD133 (Fig. 5*E*). Thus, our findings indicate that the residual cells that survived doxorubicin treatment seemed to be enriched in cancer stem cells, whereas P-BrPE eliminated the cancer stem cell population and therefore prevented tumor cell regrowth.

Effect of Glycolytic Inhibitor in Combination with DNA-damaging Agent on the Growth of Highly Tumorigenic Glioblastoma Cells in Vivo—Based on the observation that inhibition of glycolysis could preferentially kill stem-like cancer cells and prevent regrowth of residual cells *in vitro*, we then used an *in vitro-in vivo* coupled assay to further test the ability of P-BrPE to kill the tumor-initiating cells in the U87-SC population, using tumor growth in athymic mice as an *in vivo* read out for tumor initiating capacity. As shown in Fig. 6*A*, U87-SC cells were first incubated with P-BrPE, doxorubicin, or their combination for 24 h under hypoxic conditions and then inoculated subcutaneously in athymic mice. The animals were then observed for tumor formation and tumor growth without further drug treatment. All of the mice were inoculated with U87-SC cells pretreated with a clinically relevant concentration of doxorubicin (50 nM) developed tumors (22/22). P-BrPE reduced the tumor incidence to 86 and 43% at 50 and 100 μM, respectively. Importantly, combination of 50 nM doxorubicin with 50 μM P-BrPE decreased the tumor incidence to 45%, which was more than the expected additive effect (86%, $p <$ 0.05). Similarly, combination of 20 μM BCNU and 100 μM P-BrPE completely inhibited tumor formation, whereas BCNU as a single agent suppressed the tumor formation by 80% (tumor incidence was four in 20). In mice that developed tumors, the initial tumor growth during the first 2 weeks was substantially delayed in the groups treated with P-BrPE or its combination with doxorubicin/BCNU (Fig. 6*A*), suggesting fewer tumor-initiating cells left after P-BrPE treatment. Once the tumors were established, their growth trend became similar.

To test the *in vivo* antitumor activity of this therapeutic strategy, we inoculated U87-SC cells (without drug treatment) subcutaneously into athymic mice, waited for the formation of visible tumors (1 week), and then randomized the mice into six groups for treatment with P-BrPE, doxorubicin, BCNU, or their combinations. As shown in Fig. 6*B*, tumors in the control group

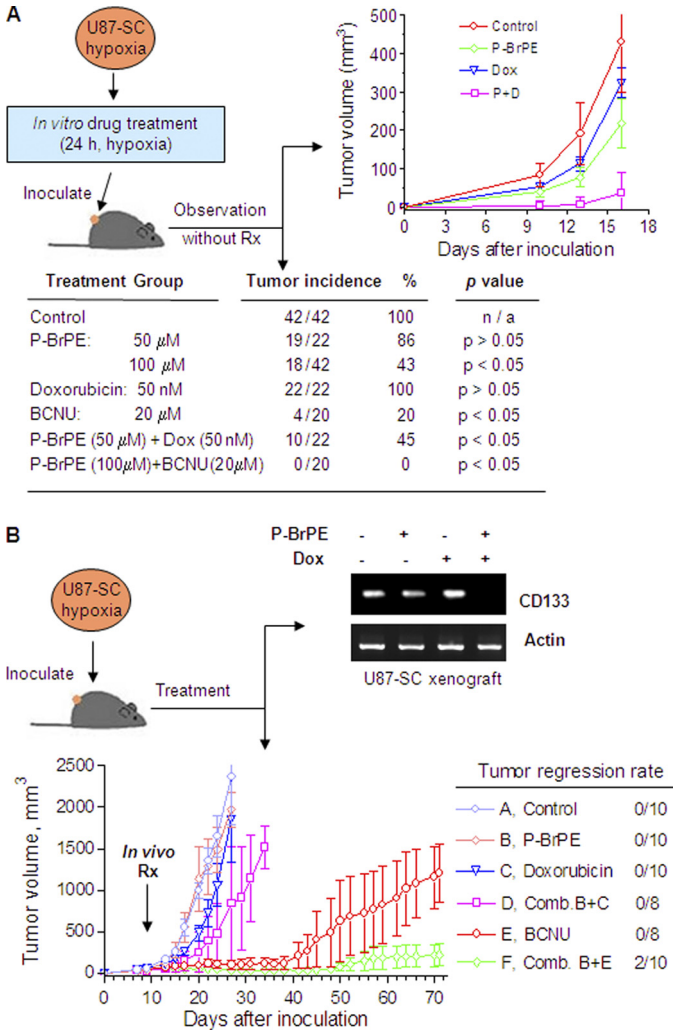

FIGURE 6. **Glycolytic inhibition suppressed tumor formation in combination with doxorubicin and BCNU in mice bearing U87-SC xenografts.** *A*, glycolytic inhibition abolished U87-SC cell (hypoxia-maintained in spheroids) tumor formation in athymic mice after a 24-h pretreatment of P-BrPE, doxorubicin (*Dox*), BCNU, and their combinations. 3×10^5 cells were inoculated per site subcutaneously into athymic mice. The table showed the tumor incidence, and the chart showed the growth curve of tumor xenograft. *B*, inhibitory effect of P-BrPE, doxorubicin (*Dox*), BCNU, and their combinations on hypoxia-maintained U87-SC tumor xenograft growth. 3×10^5 cells were inoculated per site subcutaneously on both flanks ($n = 5$). Treatment started at day 7 when tumors were visible. Two tumors in the p-BrPE + BCNU group achieved complete tumor remission (two of 10 tumors). RNA from tumor xenografts isolated from groups A–D on day 24 was extracted for analysis of CD133 expression by RT-PCR. Pooled samples of three specimens were used. The tumors in groups E and F were not analyzed for CD133 expression because of the lack of sufficient tissues (slow tumor growth) at the time of analysis when the tumors of the control mice reached maximum tumor sizes at week 4.

grew rapidly and reached the maximal size allowed by the animal research protocol within 4 weeks after inoculation. Doxorubicin (2 mg/kg) or P-BrPE (20 mg/kg) alone did not exhibit significant inhibitory effect on tumor growth. However, their combination showed a substantial retardation of tumor growth. Analysis of the stem cell marker CD133 expression in the tumor tissues by RT-PCR showed that the expression of CD133 was almost undetectable after the mice were treated with a combination of P-BrPE + Dox. This was consistent with the observation *in vitro* (Fig. 5*E*). BCNU at the dose of 20 mg/kg exhibited inhibitory effect on tumor growth but did not induce complete

regression of the tumors, which started to grow after 5 weeks. Combination of P-BrPE (20 mg/kg) and BCNU (20 mg/kg) not only effectively inhibited tumor growth but also induced complete tumor regression in two of 10 tumors in this treatment group. It is likely that this drug combination effectively killed cancer cells in the tumor bulk, as well as cancer stem cells in their hypoxic niches, leading to complete elimination of the entire tumor.

DISCUSSION

In this study, we showed that highly tumorigenic brain tumor cells with stem-like properties had low mitochondrial respiration and high aerobic glycolysis, displaying the Warburg effect. Activation of mitochondria oxidatative phosphorylation seems important for normal tissue stem cell differentiation (31, 32). Our data suggest that the stemness of cancer cells is plastic and can be influenced by microenvironment or the niche factors that suppress mitochondria activity and shift cellular energy metabolisms to glycolysis. The major mitochondrial suppression in the stem-like U87-SC cells likely occurred in the respiratory chain complex II (Fig. 4*B*), which was in part due to a decrease in SDHB expression (Fig. 4*A*). The decrease in mitochondrial respiration was compensated by a significant increase in glycolysis to maintain sufficient ATP production. Overall, our findings in the U87-SC model are consistent with the hypothesis of Warburg (20), who suggested that mitochondrial injury and increased aerobic glycolysis were important for cancer development.

This metabolic alteration seems associated with a deregulation of HIF-1α and HIF-2α. The HIF proteins play critical roles in regulating mitochondrial function and cellular metabolism and maintaining cellular stemness (33). Recent studies showed that HIF stabilization is possibly through disabling prolyl dehydrogenase as a direct consequence of succinate accumulation or indirect consequence of a ROS-mediated mechanism resulted from mitochondria complex II defect (28, 34, 35). In the U87-SC cells, it seems that the deregulation of HIF-1α and HIF-2α proteins is ROS-dependent, because the antioxidant NAC significantly enhanced the HIF protein degradation in U87-SC cells without altering mitochondria oxygen consumption activity. Our study also suggests that the increased ROS might be generated through the dysfunctional mitochondrial electron transport chains and consequently played an important role in promoting HIF-mediated up-regulation of glycolytic activity in these highly tumorigenic cancer cells. Notably, our data on HIF-1α and HIF-2α mRNA and protein levels under normoxia and hypoxia conditions suggest that HIF-1α is sensitive to ROS, whereas HIF-2α is responsive to both ROS and oxygen. However, these two homologues seem to be under differential regulation mechanisms in hypoxia conditions that is worthy of further studies.

Importantly, our study suggested that a hypoxic microenvironment seems to promote the maintenance of the tumor-initiating and stem-like properties of U87-SC cells. This observation is consistent with several other studies suggesting that hypoxic conditions enhance the *in vitro* maintenance and expansion of stem cells (12, 13). It is thought that the local oxygen levels might directly influence stem cell proliferation and differentiation and that stem cells might benefit from hypoxic conditions where oxidative DNA damage may be reduced (33). Hematopoietic stem cells seem to prefer a hypoxic niche as shown in mice where the stem cells and their supporting cells were located in the regions with the lowest oxygen tension in bone marrow (5). However, currently the influence of the microenvironment on cancer stem cells and their preferred niches still remain somewhat controversial. In contrast with the notion that the stem cell niche is hypoxic, some studies suggested that certain stem cells might reside in the vascular-rich tissue environment, where oxygen may be relatively more abundant (36, 37). It should be noted that even at the perivascular location, the actual oxygen tension may still be substantially lower than that in the ambient atmosphere, depending on the vascular types and tissue locations. In fact, under physiological conditions, the cerebral oxygen tension seems to fall within the range of hypoxic conditions (2% or 22 mmHg) used in our study (24). Thus, more studies are required to reveal the oxygen content in the microenvironment of the *in vivo* stem cell niche.

In study of normal neural stem cells, serum-free medium supplemented with certain growth factors is commonly used in maintaining stem cell culture. Because the presence of serum in the culture medium can stimulate stem cell proliferation and differentiation (38), withdrawing serum from the medium may help maintain the stem cells in their undifferentiated stage, which is important for the subsequent studies of normal stem cell differentiation and the biology-associated lineage commitment under various conditions. It has been shown that stem-like tumor cells derived from human glioblastomas cultured in serum-free medium with EGF and basic FGF more closely resemble the phenotype and the gene expression profiles of the primary glioblastomas, compared with the cells maintained long term in regular culture supplemented with 10% serum (39). However, in our U87-SC model, the use of serum-free medium seemed not an absolute requirement for the maintenance of tumor-initiating cell properties, as reflected by their expression of neural stem cell markers CD133 and nestin and their ability to form neural sphere-like structure and to form intracranial tumor with infiltrating growth. On the other hand, our data suggest that *in vivo* selection and *in vitro* culture conditions could play important role in reprogramming mitochondrial respiratory function, cellular energy metabolism, and the plasticity of stemness.

The preference of U87-SC cells on the glycolytic pathway to generate ATP suggested a novel notion that the stem-like cancer cells might be vulnerable to glycolytic inhibition. It is interesting to note that treatment of U87-SC cells with doxorubicin resulted in an enrichment of CD133-expressing cells in the surviving subpopulation, whereas incubation with 3-BrPE led to a substantial decrease of CD133 expression (Fig. 5*B*). These data suggest that these two compounds may preferentially kill two different subpopulations, with 3-BrPE killing the stem-like cancer cells and doxorubicin impacting on the progeny. As such, to effectively eliminate all tumor cells, it is important to combine conventional anticancer agents that are effective in killing the bulk of tumor cells with glycolytic inhibitors capable of killing stem-like cancer cells that are resistant to standard drugs used

in the clinic. Taken together, our study provided a biochemical basis for developing new therapeutic strategies to use novel drug combination to reduce tumor bulk and eliminate tumor-initiating cells so that better therapeutic outcomes may be achieved in cancer treatment.

Acknowledgments—We thank E. F. Hollingsworth for assistance with processing tumor tissue, K. Dunner, Jr., for processing EM samples, and Vivia V. Rubila for technical support.

REFERENCES

1. Al-Hajj, M., Wicha, M. S., Benito-Hernandez, A., Morrison, S. J., and Clarke, M. F. (2003) *Proc. Natl. Acad. Sci. U.S.A.* **100,** 3983–3988
2. Lapidot, T., Sirard, C., Vormoor, J., Murdoch, B., Hoang, T., Caceres-Cortes, J., Minden, M., Paterson, B., Caligiuri, M. A., and Dick, J. E. (1994) *Nature* **367,** 645–648
3. Singh, S. K., Clarke, I. D., Terasaki, M., Bonn, V. E., Hawkins, C., Squire, J., and Dirks, P. B. (2003) *Cancer Res.* **63,** 5821–5828
4. Zhou, S., Schuetz, J. D., Bunting, K. D., Colapietro, A. M., Sampath, J., Morris, J. J., Lagutina, I., Grosveld, G. C., Osawa, M., Nakauchi, H., and Sorrentino, B. P. (2001) *Nat. Med.* **7,** 1028–1034
5. Parmar, K., Mauch, P., Vergilio, J. A., Sackstein, R., and Down, J. D. (2007) *Proc. Natl. Acad. Sci. U.S.A.* **104,** 5431–5436
6. Guzman, M. L., Swiderski, C. F., Howard, D. S., Grimes, B. A., Rossi, R. M., Szilvassy, S. J., and Jordan, C. T. (2002) *Proc. Natl. Acad. Sci. U.S.A.* **99,** 16220–16225
7. Bao, S., Wu, Q., McLendon, R. E., Hao, Y., Shi, Q., Hjelmeland, A. B., Dewhirst, M. W., Bigner, D. D., and Rich, J. N. (2006) *Nature* **444,** 756–760
8. Al-Hajj, M. (2007) *Curr. Opin. Oncol.* **19,** 61–64
9. Jordan, C. T., Guzman, M. L., and Noble, M. (2006) *N. Engl. J. Med.* **355,** 1253–1261
10. Pardal, R., Clarke, M. F., and Morrison, S. J. (2003) *Nat. Rev. Cancer* **3,** 895–902
11. Spradling, A., Drummond-Barbosa, D., and Kai, T. (2001) *Nature* **414,** 98–104
12. Cipolleschi, M. G., Dello Sbarba, P., and Olivotto, M. (1993) *Blood* **82,** 2031–2037
13. Morrison, S. J., Csete, M., Groves, A. K., Melega, W., Wold, B., and Anderson, D. J. (2000) *J. Neurosci.* **20,** 7370–7376
14. Ezashi, T., Das, P., and Roberts, R. M. (2005) *Proc. Natl. Acad. Sci. U.S.A.* **102,** 4783–4788
15. Covello, K. L., Kehler, J., Yu, H., Gordan, J. D., Arsham, A. M., Hu, C. J., Labosky, P. A., Simon, M. C., and Keith, B. (2006) *Genes Dev.* **20,** 557–570
16. Gustafsson, M. V., Zheng, X., Pereira, T., Gradin, K., Jin, S., Lundkvist, J., Ruas, J. L., Poellinger, L., Lendahl, U., and Bondesson, M. (2005) *Dev. Cell* **9,** 617–628
17. DeAngelis, L. M. (2001) *N. Engl. J. Med.* **344,** 114–123
18. Jensen, R. L. (2009) *J. Neurooncol.* **92,** 317–335
19. Hölzer, T., Herholz, K., Jeske, J., and Heiss, W. D. (1993) *J. Comput. Assist. Tomogr.* **17,** 681–687
20. Warburg, O. (1956) *Science* **123,** 309–314
21. Jiang, H., Gomez-Manzano, C., Aoki, H., Alonso, M. M., Kondo, S., McCormick, F., Xu, J., Kondo, Y., Bekele, B. N., Colman, H., Lang, F. F., and Fueyo, J. (2007) *J. Natl. Cancer Inst.* **99,** 1410–1414
22. Xu, R. H., Pelicano, H., Zhou, Y., Carew, J. S., Feng, L., Bhalla, K. N., Keating, M. J., and Huang, P. (2005) *Cancer Res.* **65,** 613–621
23. Hamburger, A. W., and Salmon, S. E. (1977) *Science* **197,** 461–463
24. Moppett, I. K., and Hardman, J. G. (2007) *Anesth. Analg.* **105,** 1094–1103
25. Reynolds, B. A., Tetzlaff, W., and Weiss, S. (1992) *J. Neurosci.* **12,** 4565–4574
26. Slater, T. F., Sawyer, B., and Straeuli, U. (1963) *Biochim. Biophys. Acta* **77,** 383–393
27. Gottlieb, E., and Tomlinson, I. P. (2005) *Nat. Rev. Cancer* **5,** 857–866
28. Guzy, R. D., Sharma, B., Bell, E., Chandel, N. S., and Schumacker, P. T. (2008) *Mol. Cell. Biol.* **28,** 718–731
29. Gao, P., Zhang, H., Dinavahi, R., Li, F., Xiang, Y., Raman, V., Bhujwalla, Z. M., Felsher, D. W., Cheng, L., Pevsner, J., Lee, L. A., Semenza, G. L., and Dang, C. V. (2007) *Cancer Cell* **12,** 230–238
30. Geschwind, J. F., Ko, Y. H., Torbenson, M. S., Magee, C., and Pedersen, P. L. (2002) *Cancer Res.* **62,** 3909–3913
31. Parker, G. C., Acsadi, G., and Brenner, C. A. (2009) *Stem Cells Dev.* **18,** 803–806
32. Prigione, A., Fauler, B., Lurz, R., Lehrach, H., and Adjaye, J. (2010) *Stem Cells* **28,** 721–733
33. Keith, B., and Simon, M. C. (2007) *Cell* **129,** 465–472
34. Selak, M. A., Armour, S. M., MacKenzie, E. D., Boulahbel, H., Watson, D. G., Mansfield, K. D., Pan, Y., Simon, M. C., Thompson, C. B., and Gottlieb, E. (2005) *Cancer Cell* **7,** 77–85
35. Dahia, P. L., Ross, K. N., Wright, M. E., Hayashida, C. Y., Santagata, S., Barontini, M., Kung, A. L., Sanso, G., Powers, J. F., Tischler, A. S., Hodin, R., Heitritter, S., Moore, F., Dluhy, R., Sosa, J. A., Ocal, I. T., Benn, D. E., Marsh, D. J., Robinson, B. G., Schneider, K., Garber, J., Arum, S. M., Korbonits, M., Grossman, A., Pigny, P., Toledo, S. P., Nosé, V., Li, C., and Stiles, C. D. (2005) *PLoS Genet.* **1,** 72–80
36. Calabrese, C., Poppleton, H., Kocak, M., Hogg, T. L., Fuller, C., Hamner, B., Oh, E. Y., Gaber, M. W., Finklestein, D., Allen, M., Frank, A., Bayazitov, I. T., Zakharenko, S. S., Gajjar, A., Davidoff, A., and Gilbertson, R. J. (2007) *Cancer Cell* **11,** 69–82
37. Zannettino, A. C., Paton, S., Arthur, A., Khor, F., Itescu, S., Gimble, J. M., and Gronthos, S. (2008) *J. Cell. Physiol.* **214,** 413–421
38. Gage, F. H., Ray, J., and Fisher, L. J. (1995) *Annu. Rev. Neurosci.* **18,** 159–192
39. Lee, J., Kotliarova, S., Kotliarov, Y., Li, A., Su, Q., Donin, N. M., Pastorino, S., Purow, B. W., Christopher, N., Zhang, W., Park, J. K., and Fine, H. A. (2006) *Cancer Cell* **9,** 391–403